At 300 sec after a simulated Earth re-entry, the cover panels on opposite sides and between ribs 9 and 10 are heated symmetrically to the temperatures depicted in Fig. 2. As with many of the major general-purpose finite element programs employed, such as those described in Refs. 3–5, each element may be assigned only a single temperature and yields only an average thermal stress for the entire panel. However, as will be shown for the subject problem, average stress results for the associated thermal gradients are entirely unacceptable.

The finite element spanwise strains computed at the panel edges and midpoints of the section in question, compared with those obtained using classical beam theory (plane sections remain plane) were found to be in excellent agreement. Use of beam theory, for comparison purposes, appears justified for the cross section in question, as it is located reasonably outboard from the fin's root attachment section.

The corresponding finite element average membrane stresses calculated by the method presented in Ref. 6, when compared to their beam-theory counterparts, are found to mask critical stress variations within a given element (see Fig. 3). It should be noted that Webber,[7] working with uniform and variable temperature plate membrane elements, came to a similar conclusion. He found that deflections caused by heating were "acceptable" but "special attention" was necessary for "interpolation of the stresses, which could deviate considerably from the true stress state." As may be seen, however, the corresponding stresses computed by the proposed modified approach, also shown in Fig. 3, agree quite well with the beam-theory-based results. The thermal stresses in the chordwise direction are negligible because the cover corrugations permit free thermal straining.

While it may be argued that the uniform temperature elements used in this example are too "primitive," the point is made that the proposed method intrinsically yields more accurate stresses than the conventional approach, regardless of how sophisticated the element employed is.

Conclusions and Recommendations

It has been shown by means of a specific example and through general reasoning [Eqs: (1–5)], that the strains which occur as a result of structural heating are less sensitive to local temperature variations than their corresponding thermally induced stresses. Based upon this observation, an improvement over the conventional method for determining thermal stresses employing finite element procedures has been suggested. The technique proposed is equally applicable to a variety of approximate numerical procedures based upon a displacement formulation such as finite differences and other Ritz-type methods. However, the development and example treated have been based upon the finite element method, which is in popular usage because of its flexibility and efficiency in treating complex engineering structures.

Unfortunately, as of this writing, general structural analysis programs such as those described in Refs. 3–5 and 8 do not explicitly output corner or average strains. Thus, implementation of the proposed approach is, at best, awkward. Therefore, it is recommended that such programs be extended to provide a strain print-out option to facilitate the calculation of more accurate thermal stresses.

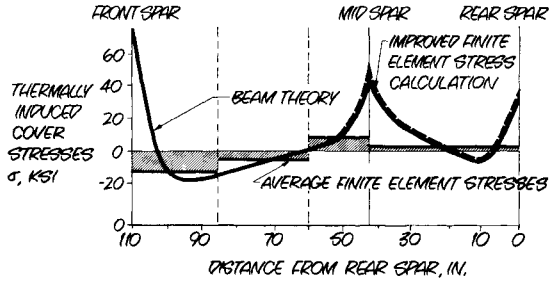

Fig. 3 Improved finite element fin cover stresses between ribs 9 and 10 vs beam theory and average finite element stresses.

References

[1] Przemieniecki, J. S., *Theory of Matrix Structural Analysis*, McGraw-Hill, New York, 1968, pp. 62–64.

[2] Ojalvo, I. U., "Thermal Dynamic Modeling Study," CR-2125, Oct. 1972, NASA.

[3] MacNeal, R. H., ed., *The NASTRAN Theoretical Manual*, NASA SP-221 (01), April 1972, p. 3.6-3.

[4] *Grumman IDEAS Manual*, Grumman Aerospace Corp., Bethpage, N.Y., Aug. 1968, Chaps. 7 and 27.

[5] Mallett, R. H. and Jordan, S., "MAGIC: An Automated General Purpose System for Structural Analysis," Contract Report for the Air Force, AFFDL-TR-68-56, Jan. 1969, Bell Aerosystems, Buffalo, N.Y.

[6] *Space Shuttle Orbiter TPS Test Bed Design*, Vol. 1, Contract Rept. 71-206-F-NAS, prepared for NASA under Contract NAS 9-12315, April 30, 1972, Grumman Aerospace Corp., Bethpage, N.Y.

[7] Webber, J. P. H., "Thermo-Elastic Analysis of Rectangular Plates in Plane Stress by the Finite-Element Displacement Method," *Journal of Strain Analysis*, Vol. 2, No. 1, 1967, pp. 43–51.

[8] Meijers, P., "Review of the ASKA Programme," Paper II-1 presented at the ONR Symposium on Numerical and Computer Methods in Structural Mechanics, Sept. 1971, Univ. of Illinois at Urbana, Urbana, Ill.

Shock Tube for Generating Weak Shock Waves

W. GAREN,* R. SYNOFZIK,* AND A. FROHN†
Technische Hochschule Aachen, Germany

THE purpose of the present Note is to introduce a new pneumatic valve which can be used to replace the diaphragm of a conventional shock tube. This device which can be opened practically independently of the pressure difference between driver gas and test gas is particularly useful for generating weak shock waves.

The principle of this device is shown in Fig. 1. The end of tube A is shut off by a rubber disk R. By increasing the

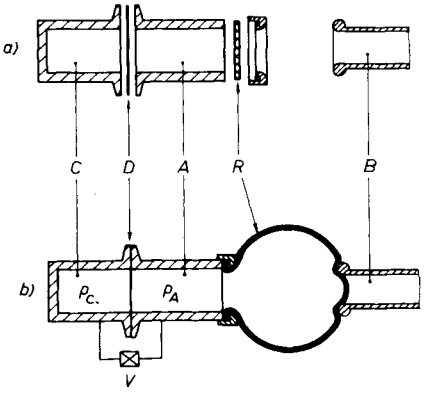

Fig. 1 Principle of pneumatic device.

Received May 24, 1973; revision received February 21, 1974.
Index category: Shock Waves and Detonations.
* Graduate Assistant.
† Professor.

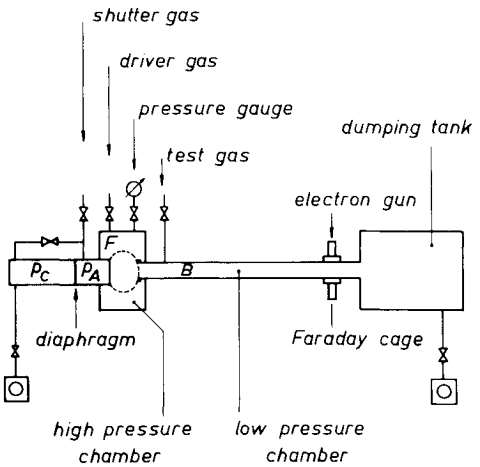

Fig. 2 Shock tube with pneumatic device.

pressure p_A the initially plane rubber disk bulges and finally provides a vacuum tight seal for tube B (Fig. 1b). During this operation valve V is open so that always $p_C = p_A$ and breaking of the diaphragm D is avoided. In order to open tube B very fast one has to lower the pressure p_A suddenly. This can be done conveniently by lowering the pressure p_C in chamber C by means of a mechanical vacuum pump until the pressure difference $p_A - p_C$ is sufficient to break the diaphragm D. In Fig. 2 it is shown how the pneumatic device is used to replace the diaphragm of a shock tube. It is assumed that all chambers are evacuated at the beginning of an experiment. By raising simultaneously the pressures p_A and p_C a vacuum tight seal is obtained between the low-pressure section B and the high pressure section F of the shock tube. After admission of driver gas and test gas the pressure p_C is lowered with a mechanical pump until the diaphragm breaks spontaneously. After rupture of the diaphragm expansion waves travel into chamber A and the rubber sheet is pulled back. In the present Note the diameter of tube A was 5 cm.

The pneumatic device has been tested in combination with two shock tubes. The first shock tube had a square cross section with inner dimensions of 1.8 cm × 1.8 cm. The second shock tube had a circular cross section with an inner diameter of 3.6 cm. The length of the low pressure section was 2.39 m for the first tube and 3.48 m for the second tube. The rubber sheet had a thickness of 2 mm. Hostaphan‡ sheet with a thickness of 50×10^{-3} mm has been used as diaphragm. Using two laser beams and phototransistors as light detectors, it has been found

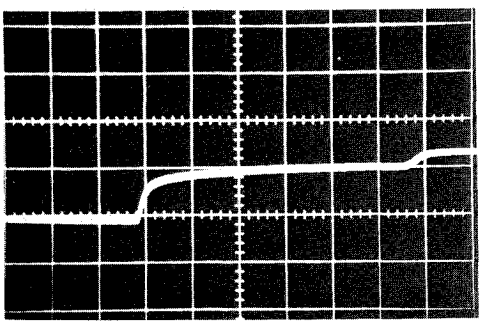

Fig. 3 Transmitted current of electron beam for shock wave in argon: $M = 1.7$, initial pressure $p_B = 3.5 \times 10^{-1}$ torr (argon), driver pressure $p_F = 40$ torr (argon), vertical scale 10 mv/cm, horizontal scale 20×10^{-6} sec/cm. First rise: shock wave, second rise: contact surface.

‡ Producer: Kalle AG, Germany.

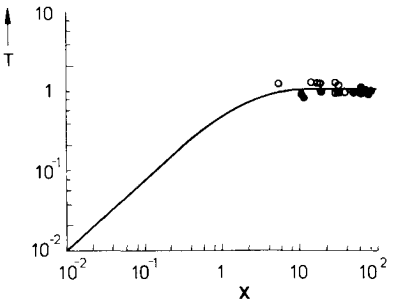

Fig. 4 Dimensionless test time T as a function of dimensionless distance X. Line is theoretical result given by Eq. (1). Open points: shock tube with cross section of 1.8 cm × 1.8 cm; closed points: shock tube with circular cross section 3.6 cm.

that 460×10^{-6} sec were needed to remove the rubber sheet 17 mm from the end of tube B. The speed of the shock wave was measured with glow discharge probes.[1] Electron beam absorption measurements have been performed with an electron gun and a Faraday cage as detector for the transmitted current.[2] The electron gun has been calibrated by varying the pressure in the low-pressure section under stationary conditions. In Fig. 3 an oscilloscope record of the transmitted electron current is shown for a shock wave in argon. The first steep rise on the oscillogram is caused by the shock front. The slow density increase behind the shock front is due to the boundary-layer growth which is appreciable because of the low test gas pressures used in the present work. The second steep density rise is interpreted as contact surface. In order to establish this, the experimental results of the time between shock front and contact surface are compared with Mirels' theoretical results[3] for the test time in low-pressure shock tubes. The dimensionless test time $T = \tau_t M a_1 / l_m$ has been plotted in Fig. 4 against the dimensionless distance $X = (T + x/l_m)\ \rho_1/\rho_2$. Here a_1 is the velocity of sound ahead of the shock, l_m the asymptotic length of the test gas column as given by Fig. 6 of Ref. 3, X is the distance between the diaphragm and the test section, and ρ_2/ρ_1 is the density ratio across the shock. According to Ref. 3, the relation between X and T is given with sufficient accuracy by

$$X = 2[-\ln(1 - T^{1/2}) - T^{1/2}] \qquad (1)$$

which relation is also plotted in Fig. 4. The agreement between experiment and theory is close enough to make the interpretation of the oscillogram acceptable.

In order to show that the first steep density rise on the oscillogram is really a shock wave and not just a compression vave the maximum slope thickness of the density profile has

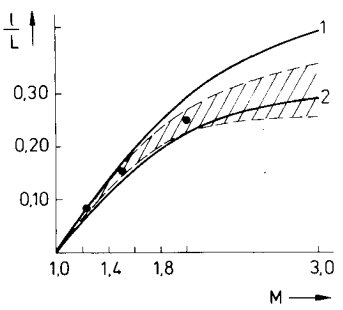

Fig. 5 Reciprocal maximum slope shock wave thickness nondimensionalized with mean free path l ahead of the shock as a function of shock Mach number M. Closed points: experimental results in the circular cross section tube of the present note; lines 1 and 2 theoretical results of Ref. 4 for Navier-Stokes equations (1) and bimodal Mott-Smith theory (2); shaded region: location of experimental results presented in Ref. 4.

been evaluated. The maximum slope thickness L is obtained from the relation

$$L = (\rho_2 - \rho_1)/(d\rho/dx)_{\max} \quad (2)$$

where ρ_1 is the density ahead of the shock, ρ_2 the density behind the shock and $(d\rho/dx)_{\max}$ the maximum slope of the density profile. The density ρ_2 is given by the Rankine-Hugoniot conditions. In Fig. 5 the experimental results for the reciprocal shock wave thickness are shown as a function of the shock Mach number M together with theoretical results based on the Navier-Stokes equations (curve 1) and on Mott-Smith's bimodal theory (curve 2). Both curves have been taken from Linzer and Hornig's paper (curves 1 and 2a in Fig. 4 of Ref. 4). The shaded region represents the location of experimental results obtained by Talbot[5,6] and Sherman with a free-molecule probe and by Linzer and Hornig[4] with the optical reflectivity method. It can be seen from Fig. 5 that the present experiments are in agreement with these experimental results.

During the test runs with the new device a few experiments have been made with a driver pressure of 1 atm and a test gas pressure of 0.1 torr. In this case the pressure difference between high-pressure section and low-pressure section was high enough to break a diaphragm of hostaphan sheet. It was therefore for these conditions possible to start the shock tube flow once with the conventional diaphragm technique and the next time with the pneumatic valve. The density histories obtained with both methods were practically identical.

The main advantages of the instrument which has been described may be summarized as follows:

1) The new device opens practically independently of the pressure difference between driver section and driven section. It becomes therefore possible to use very low driver pressures in order to obtain low shock Mach numbers.

2) The device can be opened always at exactly the same driver pressure. This means that a very good reproduction of the state of the shocked gas is possible.

3) One can always use the same gas as test gas and as driver gas because the desired shock Mach number can be adjusted with the driver pressure. This means that the driver section delivers no foreign gas into the test section during a run. The pressure increase by a shot was only a few torr in our shock tube because of the low driver pressures and the dumping tank with a volume of 1200 liter so that preparing the shock tube for the next run consisted in lowering the pressure in the driven section by a few torr and admitting the driver gas. The auxiliary diaphragm D can be exchanged very fast, because there are no particular vacuum requirements for chambers A and B. With the shock tube described here it was possible to make a run every 2 min. An additional advantage of the low driver pressures which could be used here was the reduction of the gas flow from the shock tube into the electron gun. As a consequence the lifetime of the cathode was appreciably increased.

4) The instrument may be very useful for the investigation of relaxation effects in weak shock waves which occur in the atmosphere as sonic bangs.[7]

References

[1] Bradley, J. N., *Shock Waves in Chemistry and Physics*, Wiley, New York, 1962, p. 161.

[2] Schultz-Grunow, F. and Frohn, A., "Density Distribution in Shock Waves Traveling in Rarefied Monatomic Gases," *Rarefied Gas Dynamics*, Vol. I, edited by J. H. de Leeuw, Academic Press, New York, 1965, pp. 250–264.

[3] Mirels, H., "Test Time in Low Pressure Shock Tubes," *Physics of Fluids*, Vol. 6, 1963, pp. 1201–1214.

[4] Linzer, M. and Hornig, D. F., "Structure of Shock Fronts in Argon and Nitrogen," *Physics of Fluids*, Vol. 6, 1963, pp. 1661–1668.

[5] Sherman, F. S., "Study of Shock Wave Structure and Relaxation Phenomena in Gases," TN 3298, 1955, NACA.

[6] Talbot, L. and Sherman, F. S., "Structure of Weak Shock Waves *in a Monatomic Gas*," Memo 12-14-58W, 1959, NASA.

[7] Hodgson, J. P., "Vibrational Relaxation Effects in Weak Shock Waves in Air and the Structure of Sonic Bangs," *Journal of Fluid Mechanics*, Vol. 58, Pt. 1, 1973, pp. 187–196.

A Method of Static Analysis of Shallow Shells

R. JONES*
Swinburne College of Technology, Victoria, Australia
AND
J. MAZUMDAR†
The University of Adelaide, South Australia

Introduction

THE present work may be considered as a sequel to earlier work[1-5] where a method for a large class of boundary value problems associated with the bending, buckling and vibration analysis of elastic plates and membranes of arbitrary shape was developed. These papers introduced the concept of "Lines of Equal Deflection," i.e., contour lines which are obtained by intersecting the bent plate by planes parallel to the original plane of the plate. The present Note deals with the same method as applied to shallow shells with small deflections. Many of the considerations reported in this Note are treated in greater detail in the thesis of Jones.[6] As an illustration of the method, a technically interesting example of a shallow elliptical dome is examined.

An Account of the Method

Consider an elastic isotropic shallow shell of thickness h subject to a continuously distributed normal load. Let the equation of the middle surface of the shell referred to a system of orthogonal coordinates xyz be given by

$$z = x^2/2R_x + xy/R_{xy} + y^2/2R_y \quad (1)$$

When the shell is acted upon by a transverse load $q(x, y)$ then the intersections between the deflected surface and the parallels $z = \text{const}$ yield contours which after projection onto the $z = 0$ surface are the level curves called the Lines of Equal Deflection. Denote the family of such curves by $u(x, y) = \text{const}$. If the boundary of the shell is subjected to any combination of clamping and simple support, then clearly the boundary will belong to the family of lines of equal deflection and without loss in generality we may consider that $u = 0$ on the boundary. It is clear that the lines of equal deflection form a system of nonintersecting closed curves starting from the closed boundary as one of the lines.

Consider the equilibrium of an element of the shell bounded by any contour line of constant deflection. The conditions for the equilibrium of an element of the shell require that the sum of the moments about the tangent line at any point to the curve $u(x, y) = \text{const}$ of all the forces acting on the element, and the sum of all the forces normal to the plane $z = 0$ to vanish. Therefore proceeding exactly the same way as in Ref. 1, we obtain

$$\sum M = \mathbf{n}_o \cdot \oint M_n \mathbf{n} ds + \mathbf{n}_o \cdot \oint V_n \mathbf{r}_o ds - \mathbf{n}_o \cdot \iint \left[q - \frac{N_x}{R_x} - \frac{N_y}{R_y} - \frac{2N_{xy}}{R_{xy}} \right] \mathbf{r} d\Omega = 0 \quad (2)$$

and

$$\sum Z = \oint V_n ds - \iint \left[q - \frac{N_x}{R_x} - \frac{N_y}{R_y} - \frac{2N_{xy}}{R_{xy}} \right] d\Omega = 0 \quad (3)$$

where (x_o, y_o) is a fixed point on the line $u = \text{const}$, $\mathbf{n}$ and $\mathbf{n}_o$ denote the unit vectors normal to this line at any arbitrary point (x, y) and at the fixed point (x_o, y_o), respectively, $\mathbf{r}$ and $\mathbf{r}_o$ denote the position vectors from the fixed point (x_o, y_o) to any arbitrary point inside the contour and on the contour, respectively.

Received June 8, 1973; revision received February 25, 1974.
Index category: Structural Static Analysis.

* Lecturer, Department of Civil Engineering.
† Senior Lecturer, Department of Applied Mathematics.